Numerical Investigation of Soot Reduction by Ammonia Addition in Laminar Counterflow Diffusion Flames with Reactive Inception Model

Junjun Guo, Qi Wang, Peng Liu, Erica Quadarella, S. Mani Sarathy,
William L. Roberts, Hong G. Im
Clean Combustion Research Center, Physical Sciences and Engineering Division,
King Abdullah University of Science and Technology (KAUST),
Thuwal 23955-6900, Saudi Arabia

1 Introduction

Co-firing ammonia with other fuels is receiving growing interest as a feasible solution to improve its combustion and emission properties. Many experiments found that the addition of ammonia to conventional hydrocarbon fuels can significantly reduce polycyclic aromatic hydrocarbons (PAHs) and soot formations [1-3]. However, the mechanism of soot suppression by ammonia has not been fully understood yet. The measurements [3] in premixed flames showed that the chemical compositions of nascent soot particles are similar in both ethylene and ammonia/ethylene flames. Less than 3% of chemical species are nitrogen-containing in the ammonia-doped flames. Recently, the investigations of reaction pathways [4] found that although the rate constant for the addition of HCN to aromatic structures is close to that of C_2H_2 addition, it is highly reversible at high temperatures. Therefore, the direct chemical effect of doping ammonia on PAH formation is mainly to temporarily block the reaction sites to prevent further growth of PAHs through the hydrogen abstraction acetylene addition (HACA) pathway.

Numerical simulations can provide more detail to understand the phenomena observed in experiments. However, the majority of simulations underestimated the effects of ammonia on soot reduction [2, 5, 6], which were usually explained by the inaccurate predictions of PAHs in the ammonia-diluted flames. The experimental results [1] in ammonia/ethylene counterflow diffusion flames showed that the soot sensitivity to ammonia addition was much greater than that of PAHs. Therefore, the inception model, described the transition from PAHs to soot particles, transfers the PAHs sensitivity for ammonia addition to soot particles, and this model may important for the predictions of soot sensitivity to ammonia addition.

In this study, the soot reduction by ammonia addition is numerically studied in laminar counterflow diffusion flames with a detailed gas-phase mechanism and soot aerosol dynamic model. Focusing on the soot inception model, two kinds of model framework are compared for the prediction of soot sensitivity to ammonia addition, including physical and chemical inception models.

Correspondence to: junjun.guo@kaust.edu.sa

2 Target flames

A set of laminar counterflow diffusion flames were simulated. Experiments have been performed by Bennett et al. [1] at KAUST. The fuel composition consists of ethylene diluted by nitrogen and/or ammonia while the oxidizer stream is made up of 24.95% O_2 and 75.05 N_2 in vol. The distance between fuel and oxidizer nozzles is 0.75 cm, and the global strain rate is 80 s^{-1}. Table 1 shows the experimental conditions. The soot volume fraction and PAHs signal were measured using planar laser-induced incandescence (PLII) and planar laser-induced fluorescence (PLIF) techniques, respectively.

Table 1. Experimental conditions.

	Fuel				Oxidizer		
	C_2H_4	N_2	NH_3	*U* [cm/s]	O_2	N_2	*U* [cm/s]
Case 1	75%	25.0%	0	15.0	24.95%	75.05%	15.0
Case 2	75%	19.0%	6.0%	15.0			
Case 3	75%	12.5%	12.5%	15.0			
Case 4	75%	0	25.0%	15.0			

3 Computational approach

3.1 Modeling of laminar sooting flame

Numerical simulations of laminar counterflow flames were conducted using the counterflow flame solver in OpenSMOKE++ [7]. A reduced gas-phase mechanism is used to describe gas-phase pyrolysis, oxidation, and precursors' evolution. The corresponding detailed mechanism is a combination of the KAUST-Aramco PAH 3.0 mechanism [8] and nitrogen chemistry developed by Glarborg et al. [9]. The interactions between C_0-C_2 species and nitrogen are considered. The mechanism reduction was performed using the directed relation graph (DRG) approach, DRG with error propagation (DRGEP) and DRGEP-aided sensitivity analysis. The reduced mechanism was comprehensively evaluated to ensure that it provides nearly identical results to the detailed mechanism under the target conditions.

Soot particle dynamics is handled using the hybrid method of moments (HMOM) [10]. Soot inception involves the collision of PAH dimers, which consist of a molecular cluster composed of two PAH molecules. Once formed, dimers can collide to incept the first soot particles or be adsorbed onto the soot surface. A detailed discussion of the inception model is provided in the following paragraphs. The HACA mechanism is used to describe surface growth. Finally, O_2- and OH-induced soot oxidation is considered.

3.2 Soot inception model

There are currently two main types of soot inception mechanisms [11]: (1) the process is described by physical collisions of PAHs forming dimers via van der Waals forces, usually referred to as a physical inception mechanism; (2) chemical inception in which PAH molecules combine through chemical reactions. The performances of two kinds of soot inception models are evaluated in this study. The first one is based on the framework of physical inception. The model was developed and evaluated in our previous study [12], and a brief description is given here. As shown in Fig. 1(a), the model assumes the dimers' formation through irreversible homogeneous and heterogeneous dimerization reactions via van der Waals forces. The dimerization rate constant is calculated as:

$$\omega_{phy} = \frac{1}{4} E_F \sum_{i=1}^{n} \sum_{j=i}^{n} \gamma_{i,j} \left(d_i + d_j\right)^2 [PAH_i][PAH_j] Av \sqrt{\frac{8\pi k_b T}{\mu_{i,j}}}, \quad (1)$$

where $\gamma_{i,j}$ is the sticking coefficient introduced to describe the probability of successful collisions among PAHs, which is a function of temperature and separation distance between the colliding entities.

Detailed calculation of the sticking coefficient and other variables can be found in [12]. This model is referred to as the irreversible inception model in this work.

The second one is a simplified reactive inception model based on the chemical inception framework. Since the kinetic details of the chemical inception mechanism are currently unclear, the present model should be viewed as a reasonable simplification that is amenable to CFD applications. Experiments [11] demonstrated that dimerization is a reversible reaction (R1):

$$\mathrm{PAH}_i + \mathrm{PAH}_j \leftrightarrow \mathrm{Dimer}^*_{i,j} \tag{R1}$$

The reversibility of PAHs dimerization is considered with the equilibrium constant [13]. Thermodynamic calculations showed that dimers held by van der Waals forces are not strong enough to survive at flame temperature conditions [14]. Experiments [15] in laminar diffusion flames suggested that the formation of strong carbon-carbon covalent bonds between PAHs in the dimer may be necessary to stabilize it. To avoid the complexity of detailed chemical inception mechanisms, only the dominant pathways are considered for CFD simulations. A physically-bonded dimer radical ($\mathrm{Dimer}^*_{i,j}\_1$) is formed from the physically-bonded dimer ($\mathrm{Dimer}^*_{i,j}$) via the reversible dehydrogenation reactions (R2) and (R3).

$$\mathrm{Dimer}^*_{i,j} + H \leftrightarrow \mathrm{Dimer}^*_{i,j}\_1 + H_2, \tag{R2}$$

$$\mathrm{Dimer}^*_{i,j} + OH \leftrightarrow \mathrm{Dimer}^*_{i,j}\_1 + H_2O, \tag{R3}$$

$$\mathrm{Dimer}^*_{i,j}\_1 \leftrightarrow \mathrm{Dimer}_{i,j} + H. \tag{R4}$$

The dimer radical could be stabilized by the formation of a carbon-carbon covalent bond, followed by the hydrogen abstraction as shown in the last reaction (R4). The formation of covalent bonds is a reversible process for the reaction between molecule and radical, e.g. interaction between benzene and phenyl. To obtain sufficient and meaningful carbon flux, the formation of carbon-carbon covalent bonds is assumed to be irreversible in this study. Similarly to Naseri et al. [16], steady-state assumption is made for the reversible dimerization and dehydrogenation processes, and then the steady state concentrations of $\mathrm{Dimer}^*_{i,j}$ and $\mathrm{Dimer}^*_{i,j}\_1$ can be calculated. The dimerization rate is then calculated as

$$\omega_{chem} = k_{4,f}\left[\mathrm{Dimer}^*_{i,j}\_1\right]. \tag{2}$$

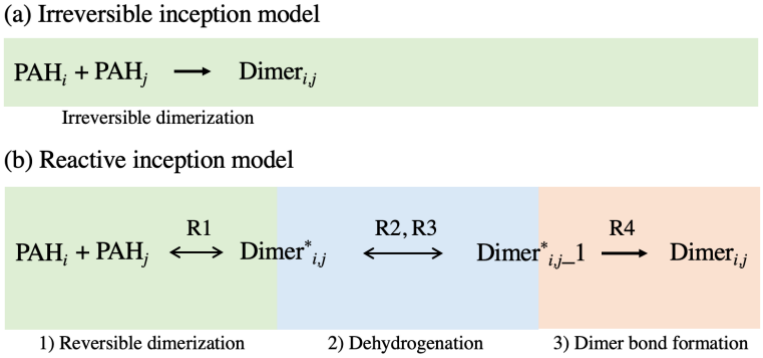

Figure 1: Soot inception model framework: (a) irreversible inception model, (b) reactive inception model

The selection of soot precursors is another key point to determine the carbon flux from the gas phase to the soot particles. A_4 is often taken as a soot precursor in soot modeling. However, the concentration of A_4 is very low and often does not provide sufficient carbon flux in some non-premixed flames [8, 12]. Therefore, smaller PAHs, such as A_2 and A_2R_5, are usually included in the set of precursors. Recent experiments [17] suggested that only small aromatics with one or two rings are present in sufficiently high concentrations to provide sufficient carbon flux through dimerization. In our previous studies [8, 12], starting from A_2, PAH species with six- and five-membered rings are used as soot precursors in the irreversible inception model. In the reactive inception model, the soot precursor pool is extended to

include A_1, A_1CH_3, A_1C_2H, and Indene. The motivation for this treatment is to provide a sufficient soot volume fraction in simulations compared to experimental data.

4 Results and discussion

The measured and predicted benzene mole fractions are shown in Fig. 2(a). The benzene was measured offline using gas chromatography-mass spectrometry. The error bars in Fig. 2(a) represent the uncertainty of repeated experiments. The measurements in each case nearly overlap. The mole fractions of benzene predicted by the two inception models are almost identical, so only the results of the reactive inception model are shown in Fig. 2(a). The simulation results are in qualitative agreement with the measurements, with the predicted peak values being about half of the measurements for all conditions.

Figure 2(b) shows the normalized peak value of the measured PAHs signal and predicted PAHs mole fraction. Generally, fluorescence from PAHs has longer wavelengths as the number of rings increases. Fluorescence from 2–3 ring PAHs is typically found in the range around 350 nm, and 3–4 ring PAHs have been shown to fluoresce at 400 nm. Larger PAHs are expected to fluoresce at 450 nm. Both measurement and simulation results show that with the increase of ammonia addition, the peak values of PAHs concentration decrease. The PAHs sensitivity to ammonia addition increases with the molecular weight of the species. The predicted sensitivity of PAHs to ammonia addition is in good agreement with the measured results.

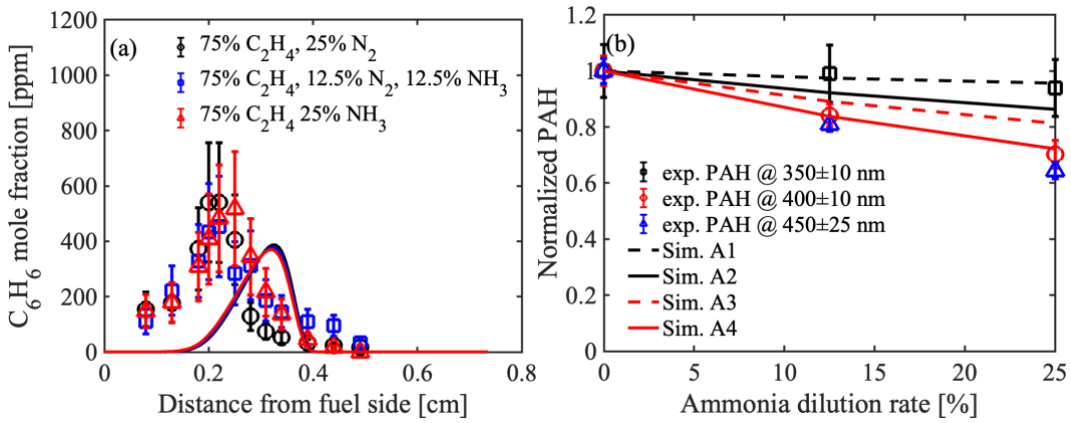

Figure 2: (a) Measured and predicted mole fractions of benzene. The measurements were divided by a factor of 2 for comparison. (b) Normalized measured peak PAHs signal and predicted peak PAHs mole fractions. The simulations used the reactive soot inception model.

The soot volume fraction profiles and normalized peak values are shown in Fig. 3. The inception model has a great effect on the peak value and spatial distribution of the soot volume fraction. Compared with the irreversible inception model, the soot distribution region predicted by the reactive inception model is wider and closer to the high-temperature region, which is consistent with the measurement. However, both nucleation models underestimate the soot volume fraction.

As shown in Fig. 3(b), both inception models underestimate the soot sensitivity to ammonia addition. Specifically, the peak soot volume fraction in the case with 25% ammonia addition is 18% of that in the case without ammonia addition. The values predicted by the reactive inception model and the irreversible inception model are 40% and 80%, respectively. The reactive inception model significantly improved the prediction of soot sensitivity to ammonia addition compared to the irreversible inception model. Although the predicted PAHs trend is consistent with the experiment, the soot sensitivity still shows inconsistencies. This suggests that the discrepancy between experiments and numerical predictions does not only originate from the gas-phase mechanism, but the existing soot models may not fully account for the effects of ammonia addition on soot formation.

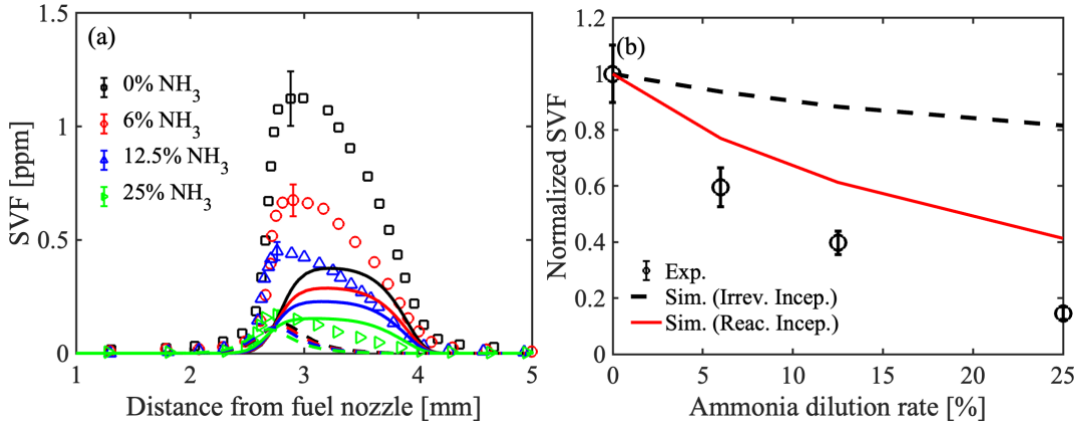

Figure 3: (a) Measured and predicted soot volume fraction (SVF) with different ammonia dilution rates. (a) Normalized peak SVF varies with ammonia dilution rate. Solid line represents the results using reactive inception model, dash line represents the results using irreversible inception model.

To understand why the reactive inception model provides better prediction of soot sensitivity to ammonia addition, the source terms of each pathway for soot formation and their sensitivity to ammonia addition are examined, and the results are shown in Fig. 4. Note that the HACA by reactive inception model (solid blue line) in Fig. 4(a) is multiplied by a factor of 0.01 for comparison. The temperature profile is also provided in Fig. 4(a) for reference. The position of the soot source term predicted by the reactive inception model is closer to the peak temperature because radicals (H and OH) mainly exist in the high-temperature region. The peaks of inception and adsorption predicted by the two inception models are similar. However, the surface growth rate controlled by the HACA mechanism differs by two orders of magnitude, because the temperature at the soot region in cases with the reactive inception model is significantly higher than that with the irreversible inception model.

In the cases using the irreversible inception model, the soot formation is mainly dominated by dimer adsorption. However, when using the reactive inception model, soot formation is dominated by surface growth controlled by the HACA mechanism. Figure 4(b) shows that the HACA source term is highly sensitive to ammonia addition, followed by dimer adsorption and finally inception. The inception and adsorption processes are mainly affected by the PAHs concentrations, while the surface growth controlled by the HACA mechanism is inhibited because of the change in the radicals concentrations, which reduce the active sites on the soot surface.

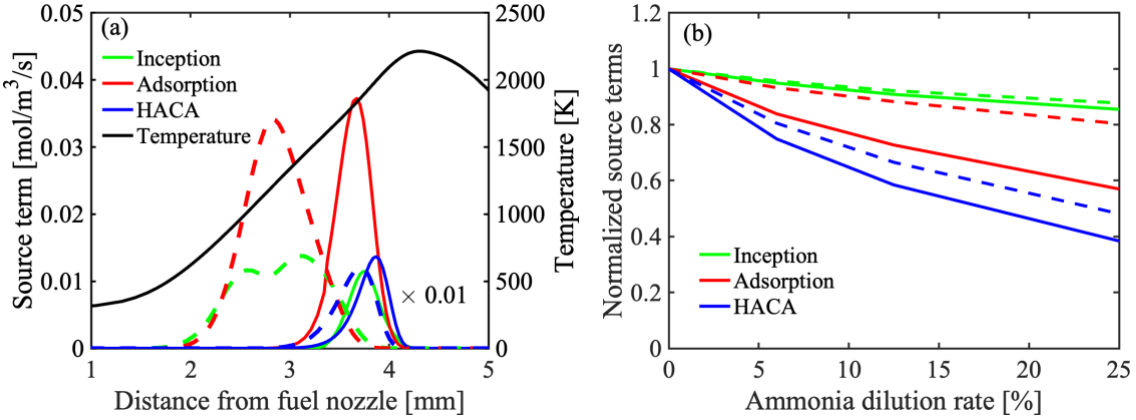

Figure 4: Predicted source terms of each pathway for soot formation, (a) source terms in the case without ammonia; (a) Normalized peak source terms in cases with different ammonia addition. Solid line represents the results using reactive inception model, dash line represents the results using irreversible inception model. Solid blue line in (a) is multiplied by a factor of 0.01 for comparison.

5 Conclusions

The suppression of soot formation by ammonia addition in ethylene laminar diffusion flames was studied numerically using a reactive soot inception model. The following conclusions are drawn:

- Compared with the irreversible soot inception model, the predictions of soot spatial distribution and sensitivity to ammonia addition have been significantly improved by the reactive inception model, because the HACA surface growth dominates soot formation.
- Concerning the soot formation pathways, the surface growth controlled by the HACA mechanism was the most sensitive to ammonia addition, followed by the dimer adsorption process, and finally soot inception.

Further numerical research will be carried out in the laminar coflow flame with the same fuel composition and ammonia dilution ratios, and the results will be presented at the colloquium.

References

[1] Bennett AM, Liu P, Li Z, Kharbatia NM, Boyette W, Masri AR, et al. (2020). Soot formation in laminar flames of ethylene/ammonia. Combust Flame. 220:210.
[2] Zhou M, Yan F, Ma L, Jiang P, Wang Y, Ho Chung S. (2022). Chemical speciation and soot measurements in laminar counterflow diffusion flames of ethylene and ammonia mixtures. Fuel. 308.
[3] Shao C, Campuzano F, Zhai Y, Wang H, Zhang W, Mani Sarathy S. (2022). Effects of ammonia addition on soot formation in ethylene laminar premixed flames. Combust Flame. 235.
[4] Wang Q, Shi X, Zhang X, Shao C, Sarathy SM. (2023). Chemistry of nitrogen-containing polycyclic aromatic formation under combustion conditions. Combust Flame. 249.
[5] Zaher MH, Chu C, Dadsetan M, Eaves NA, Thomson MJ. (2022). Experimental and numerical investigation of soot growth and inception in an ammonia-ethylene flame. Proc Combust Inst.
[6] Montgomery MJ, Kwon H, Dreyer JAH, Xuan Y, McEnally CS, Pfefferle LD. (2021). Effect of ammonia addition on suppressing soot formation in methane co-flow diffusion flames. Proc Combust Inst. 38(2):2497.
[7] Cuoci A, Frassoldati A, Faravelli T, Ranzi E. (2015). OpenSMOKE++ : An object-oriented framework for the numerical modeling of reactive systems with detailed kinetic mechanisms. Comput Phys Commun. 192:237.
[8] Guo J, Liu P, Quadarella E, Yalamanchi K, Alsheikh I, Chu C, et al. (2022). Assessment of physical soot inception model in normal and inverse laminar diffusion flames. Combust Flame. 246:112420.
[9] Glarborg P, Miller JA, Ruscic B, Klippenstein SJ. (2018). Modeling nitrogen chemistry in combustion. Prog Energy Combust Sci. 67:31.
[10] Mueller ME, Blanquart G, Pitsch H. (2009). Hybrid Method of Moments for modeling soot formation and growth. Combust Flame. 156(6):1143.
[11] Wang H. (2011). Formation of nascent soot and other condensed-phase materials in flames. Proc Combust Inst. 33(1):41.
[12] Quadarella E, Guo J, Im HG. (2022). A consistent soot nucleation model for improved prediction of strain rate sensitivity in ethylene/air counterflow flames. Aerosol Sci Technol. 56(7):636.
[13] Miller JH. (1991). The kinetics of polynuclear aromatic hydrocarbon agglomeration in flames. Symposium (International) on Combustion. 23(1):91.
[14] Totton TS, Misquitta AJ, Kraft M. (2012). A quantitative study of the clustering of polycyclic aromatic hydrocarbons at high temperatures. Phys Chem Chem Phys. 14(12):4081.
[15] Mercier X, Carrivain O, Irimiea C, Faccinetto A, Therssen E. (2019). Dimers of polycyclic aromatic hydrocarbons: the missing pieces in the soot formation process. Phys Chem Chem Phys. 21(16):8282.
[16] Naseri A, Kholghy MR, Juan NA, Thomson MJ. (2022). Simulating yield and morphology of carbonaceous nanoparticles during fuel pyrolysis in laminar flow reactors enabled by reactive inception and aromatic adsorption. Combust Flame. 237:111721.
[17] Gleason K, Carbone F, Gomez A. (2021). PAHs controlling soot nucleation in 0.101—0.811MPa ethylene counterflow diffusion flames. Combust Flame. 227:384.